Plasma Chemistry and Plasma Processing
https://doi.org/10.1007/s11090-018-9949-4

ORIGINAL PAPER

Generation of Long Laminar Plasma Jets: Experimental and Numerical Analyses

Sen-Hui Liu[1,3] · Shan-Lin Zhang[1] · Cheng-Xin Li[1] · Lu Li[2] · Jia-Hua Huang[2] · Juan Pablo Trelles[3] · Anthony B. Murphy[4] · Chang-Jiu Li[1]

Received: 29 August 2018 / Accepted: 29 November 2018

Abstract

A novel direct current non-transferred arc plasma torch that can generate silent, stable and super-long laminar plasma jets in atmospheric air is investigated. The results showed that laminar plasma jets of length ranging from 100 to 720 mm in length can be generated by controlling the gas input rate ranging from 8.5 to 15 L min^{-1} and the output power from 8.5 to 28 kW. The length of the plasma jets generally increased with the output power and gas flow rate. Observations of temporal evolution of the plasma jet appearance and the voltage demonstrated that the jet is highly stable in the atmospheric environment. The fluid dynamic properties of the laminar plasma jet were studied using a numerical simulation incorporating a laminar flow model and an RNG turbulent flow model. Simulation results show the expansion of a high temperature region close to the torch nozzle exit, corresponding to a bright region observed in experiments.

Keywords Laminar plasma jet · Voltage current characteristics · Voltage vibration · Numerical simulation

List of Symbols

C_p	Specific heat at constant pressure (J $kg^{-1}K^{-1}$)
E	Electric field (V m^{-1})
T	Temperature (K)
W	Power (W)
I	Current (A)

Electronic supplementary material The online version of this article (https://doi.org/10.1007/s11090-018-9949-4) contains supplementary material, which is available to authorized users.

✉ Cheng-Xin Li
licx@mail.xjtu.edu.cn

[1] State Key Laboratory for Mechanical Behavior of Materials, School of Materials Science and Engineering, Xi'an Jiaotong University, Xi'an 710049, Shaanxi, China

[2] Zhenhuo Plasma Technology Co., Ltd, Chendu 610065, Si Chuan, China

[3] Department of Mechanical Engineering, University of Massachusetts Lowell, Lowell, MA 01854, USA

[4] CSIRO Manufacturing, PO Box 218, Lindfield, NSW 2070, Australia

Q Gas flow rate (kg s^{-1})
k Turbulent kinetic energy (m^2 s^{-2})

Greek Symbols

ε Dissipation rate of turbulent kinetic energy (m^2 s^{-3})
ε_r Net emission coefficient (W $m^{-3}sr^{-1}$)
κ Thermal conductivity (W $m^{-1}K^{-1}$)
μ Dynamic viscosity (kg $m^{-1}s^{-1}$)
μ_t Turbulent viscosity (kg $m^{-1}s^{-1}$)
μ_{eff} Effective viscosity (kg $m^{-1}s^{-1}$)
σ Electrical conductivity (S m^{-1})
ρ Density (kg m^{-3})
ϕ Electric potential (V)

Abbreviations

LTE Local thermodynamic equilibrium
RNG Renormalization group methods
MHD Magnetohydrodynamic model
NEC Net emission coefficient

Introduction

Thermal plasmas are characterized by heavy-particle and electron temperatures of order 10^4 K, and typically operate at or near atmospheric pressure. They can be generated by electric arcs, which have high current densities, and can be transferred to the workpiece (as, for example, in arc welding, plasma cutting and other applications) or non- transferred (as, for example, in plasma spraying) [1]. In the non-transferred arc plasma torch, high temperature is achieved through a direct current (dc) arc induced between a conical cathode and an anode nozzle [2]. The arc properties depend on the internal-channel design of the torch, the type of working gas and its flow rate, the arc current and other operating parameters. The arc generates the high-temperature plasma through continuous energy dissipation of the current flowing through the gas. The plasma jet exits the torch from the anode nozzle, subsequently experiencing deceleration and cooling due to its interaction with the cold gas from the discharge environment. As a representative example, at an axial position of 100 mm from the nozzle exit, a pure argon plasma jet consists of about 80% air in an atmospheric environment [3]. The length of plasma jet in an atmospheric environment is usually less than 200 mm. Non-transferred arc plasma jets are used in deposition, gasification, waste conversion, metallurgy, some welding and cutting processes, and plasma spraying.

Arc plasma torches generally operate at high output power (25–150 kW) and high gas flow rate (usually $\geq$30 slpm) [2, 3], and generate high levels of noise to the surrounding environment ($\geq$120 dB). In the atmospheric plasma spraying process, the fluid dynamics of the plasma jet lead to the development of turbulence associated with strong entrainment of ambient gas into the plasma jet, lowering the controllability and reproducibility during the plasma spraying process [4, 5]. The fluctuation behavior of the plasma jet and the internal arc instabilities also significantly affect both torch performance and coating quality [6, 7].

An alternative type of plasma jet is the laminar plasma jet, which operates at a relatively low Reynolds number at the nozzle exit and reduces turbulent cold gas entrainment and the axial attenuation of the jet temperature and velocity. During the past three decades, several groups around the world have researched direct-current non-transferred arc plasma torches that can generate stable, long, quasi-laminar or totally laminar plasma jets. Zhukov and coworkers took the lead in designing a powerful high-enthalpy direct current plasma torch that was applied to plasma chemical technologies [1, 8]. Their design featured several linear interelectrode inserts between the cathode and the anode to extend the arc column [9].

Subsequently, a plasma torch with a much larger nozzle outlet and a jet length up to 600 mm was developed by Hamatanis of the Nippon Steel Corporation in 1999. This torch used an optimized interelectrode geometry and was used in metallic pipe butt welding and the synthesis of fine powders [10, 11].

At almost the same time, W. X. Pan and C. K. Wu from the Chinese Academy of Science designed an argon- nitrogen direct- current plasma torch that can generate a long, silent and stable plasma plume within a wide range of working parameters in either the ambient environment or in a low-pressure environment [12, 14]. The laminar plasma jet had a length up to 45 times its diameter and was applied to depositing thermal sprayed coatings and for strengthening metallic surfaces by remelting [12, 13]. Since then, researchers from Pan's group and Chen Xi's group studied the flow characteristics of this laminar plasma torch and jet using experimental and numerical simulation methods. These works included the studies of torch geometry and the voltage–current characteristics [14–16], experimental measurement of the jet flow field [17, 18] and the heat flux density of the plasma plume [19]. They performed experimental and numerical investigations of the laminar plasma jet impinging on a substrate [20–24], observations of the arc root motion in the cylindrical channel of the plasma torch [25] and two and three-dimensional modelling of laminar plasma jets with or without the entrainment of ambient air and a cylindrical shield [26–29]. These results explored the effects of natural convection and lateral particle injection on the laminar plasma jet [30, 31] and compared the performances of turbulent and laminar plasma jet using experimental and numerical analyses [28, 32]. These fundamental studies and practical achievements made huge contributions to the field of laminar plasma torch research.

In the thermal spraying research area, the huge entrainment of surrounding gas and turbulent transport in the plasma plume always occurred in atmospheric environment. The coating quality is significantly affected from the jet instabilities of the plasma torch [33]. This newly developed laminar plasma torch has significant potential for application in advanced thermal spraying processes [12, 34, 35] and other materials processing technologies [9, 11, 13].

In this work, a novel direct-current non-transferred arc plasma torch with a unique inside channel structure is presented. This torch can also generate long, silent and stable laminar plasma plumes in atmospheric environment at different gas flow rates and output powers. The fluid dynamic properties of the laminar plasma jet have been studied by a combination of experiments and numerical simulation. Experiments have been conducted to study the voltage–current and plasma jet flow characteristics under various working parameters, including the jet lengths variation, time-resolved of arc voltage fluctuation and jet plume. The numerical simulation was modelled in two-dimensional calculation domain by using Laminar model and RNG turbulent transport model.

Characteristics of Plasma Jet, Power Supply and Working Parameters

Properties of the Laminar Plasma Jets

Figure 1 shows a schematic diagram of the direct-current non-transferred laminar plasma torch (ZH-30, Zhenhuo Plasma Technology Co. Ltd., Chengdu, China) used in this study. It is composed of a cathode, insulated inserts, an anode and a nozzle outlet. The diameter of the nozzle exit is 5 mm, and the insulated inserts are assembled with several insulating rings to extend and constrict the arc column in a cylindrical channel. The length of the insulated inserts can be changed depending on the desired applications. The trumpet-like structure of the anode is, however, innovative, and leads to the specific characteristics of the plasma flow near the torch exit that are beneficial for the generation of a stable laminar plasma jet. The details of the design and the fluid dynamic characteristics inside the plasma torch are presented elsewhere [36]. The rated output power is 30 kW. The working gas is a mixture of 70% nitrogen and 30% argon by volume, unless otherwise noted. In fact, both pure argon and pure nitrogen can generate long laminar plasma jet in ambient air, although the plasma plume with this mixture is more stable and leads a longer service life in experiment.

The in situ experimental measurement of jet length in atmospheric environment are shown in Figs. 2, 3 and 4 by using the Nikon D3400 camera, regular laminar plasma jets can be generated from the laminar plasma torch under a wide range of output power and gas flow rates, producing a low-level of noise (< 80 dB) in the ambient environment. When the inlet gas rate was lower than 8.5 L min^{-1} or higher than 15 L min^{-1}, the plasma jets become uniformly short (about 80 mm) and extremely noisy (about 110 dB) because of intense entrainment of ambient air, just as in the case of conventional direct-current non-transferred arc plasma jets.

A wide range of laminar plasma jet lengths can be obtained by increasing the current from 60 to 165 A under the corresponding gas flow rate from 8.5 to 15 L min^{-1} (Fig. 5). The maximum length of the laminar plasma jet reaches 720 mm at a current of 160 A and a gas flow rate of 8.5 L min^{-1}; this is longer than the values obtained in other published studies [9, 11, 14]. At the high gas flow rate of 15 L min^{-1} and a current of 160 A, a stable laminar plasma jet with a length greater than 200 mm is also generated (Fig. 3b). As shown in Fig. 4, the length of the laminar plasma jet decreased approximately monotonically with increasing gas flow rate at a given current. The laminar plasma jets at a current of 160 A

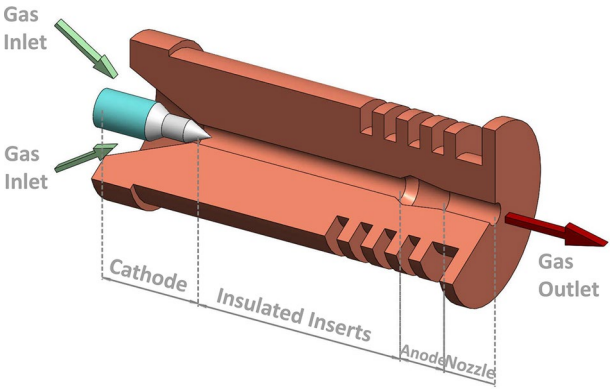

Fig. 1 Schematic diagram of internal structure of the laminar plasma torch

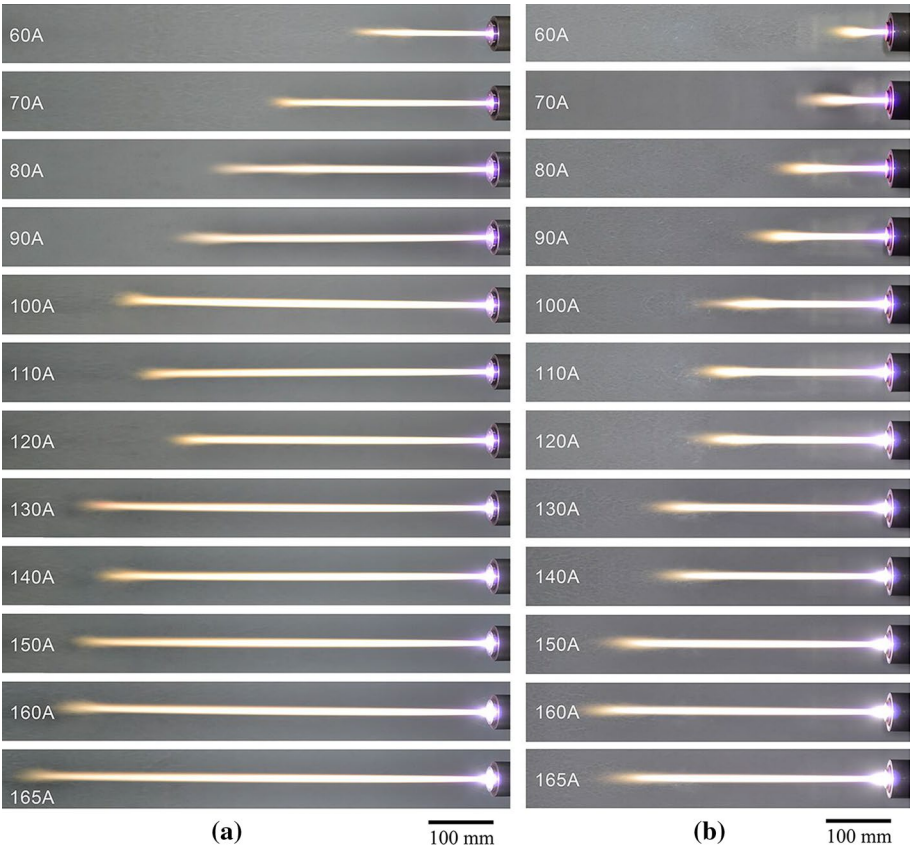

Fig. 2 Laminar plasma jet, showing variation in length for different working current. **a** Gas flow rate of 8.5 L min^{-1}; **b** gas flow rate of 11.5 L min^{-1}

(Fig. 4b) were all longer than those at a working current of 100 A (Fig. 4a) for every gas flow rate investigated, suggesting that the higher output power associated with the higher current increases the nozzle exit temperature and velocity.

A bright emission region appears in the vicinity of the nozzle orifice at higher gas flow rates and output power. The time-resolved voltage fluctuations during the laminar plasma torch operation are shown in Fig. 6. (The voltage was measured using a TPS-2000 probe manufactured by Tektronix Inc. USA). The voltage fluctuation values were confined within a range of between ± 0.5 and ± 2 V, depending on the operating conditions, which was significantly lower than those found in other commercial non-transferred arc plasma torches under higher voltage fluctuation conditions (voltage fluctuations are usually in the range of ± 5 V up to about ± 20 V) [5, 37]. Relatively low voltage fluctuations were also observed with the laminar plasma torch of W. X. Pan et al. [14].

The time-dependent stability of the arc plasma jet were monitored using a high-speed micro-lens camera (Nikon AF MICRO 200 mm) at the nozzle exit. The jet was found to be quite stable, as shown in Fig. 7 and the supplementary video file. The stability in an atmospheric environment will be useful for application to plasma processes such as deposition, welding, surface hardening and to provide a substantially improved working environment.

Fig. 3 Laminar plasma jet, showing variation in length for different working current. **a** Gas flow rate of 14 L min^{-1}; **b** gas flow rate of 15 L min^{-1}

Arc Voltage–Current Characteristics Under Various Conditions

Arc Voltage Current Characteristics in Different Gas Mixtures

The chosen working gas was a nitrogen and argon mixture, with pure argon used to start the arc, and pure nitrogen as the secondary gas to obtain a longer laminar plasma jet. Argon is a monatomic inert gas with low thermal conductivity and energy density. Its use is beneficial for the service time of the electrode and nozzle as its use limits the heat transfer to the edge regions. Nitrogen has much higher thermal conductivity and power density than

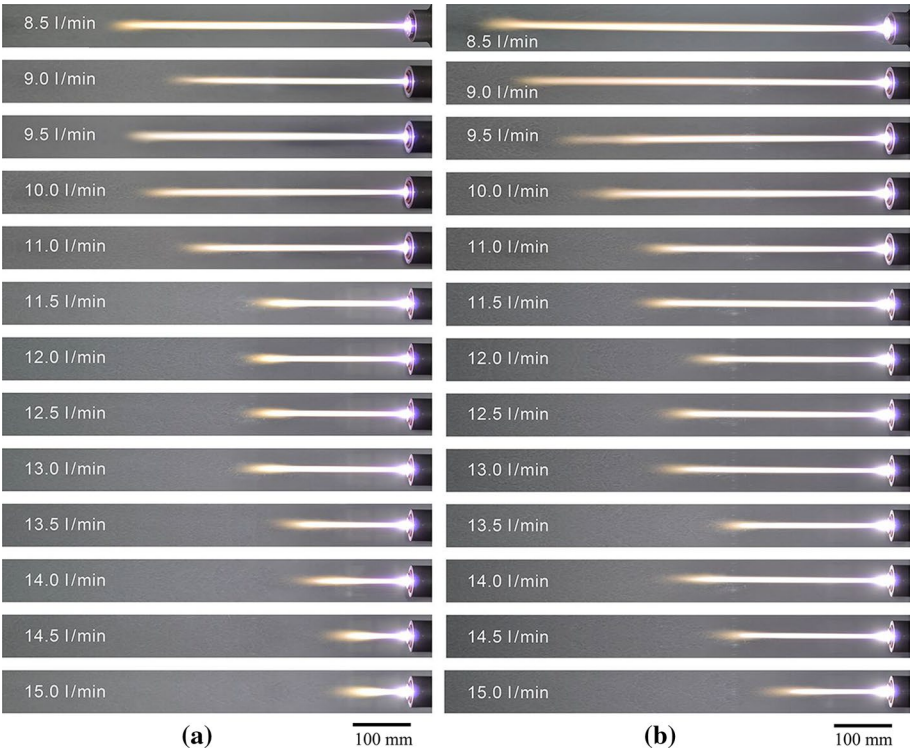

Fig. 4 Laminar plasma jet, showing variation in length for different gas flow rates. **a** I = 100 A; **b** I = 160 A

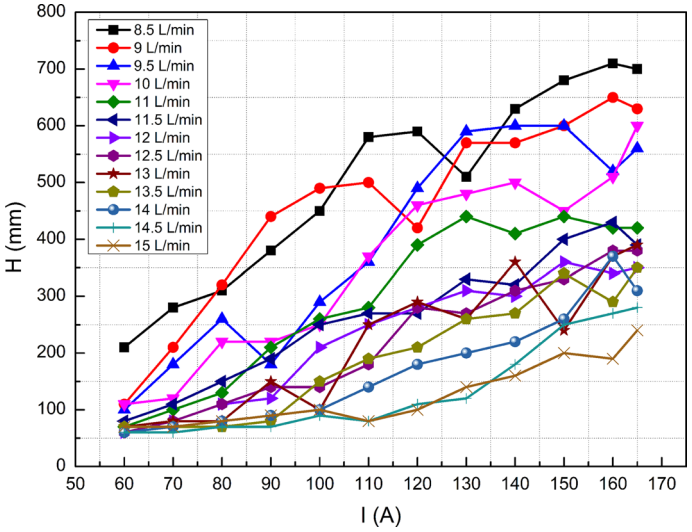

Fig. 5 Dependence of laminar plasma jet length on arc current for different gas flow rates

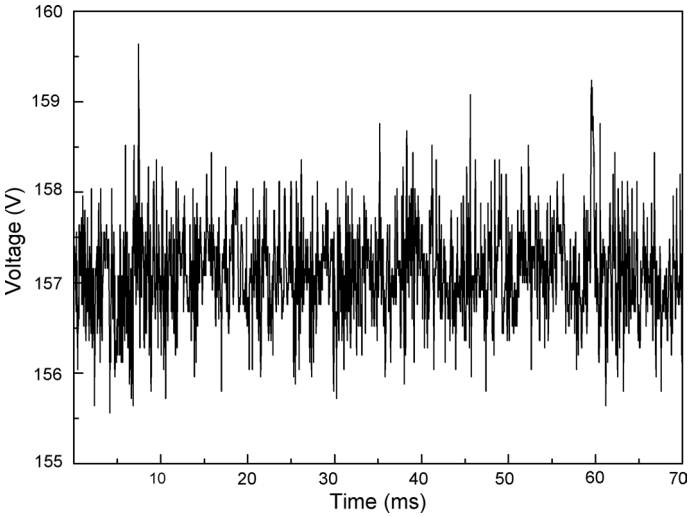

Fig. 6 Time-resolved arc voltage at the working current of 160 A and gas flow rate of 14 L min^{-1}

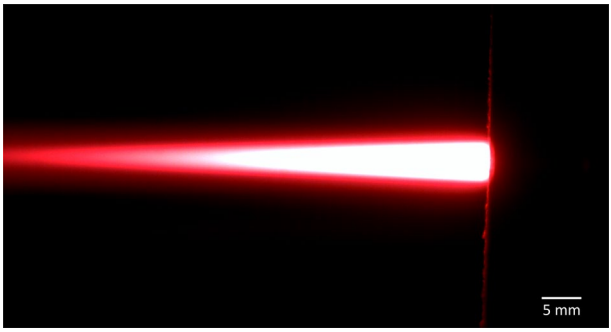

Fig. 7 Photo showing the nozzle exit part of a long laminar plasma jet obtained with a high-speed micro-lens camera with exposure time of 1/200 s (I = 160 A, gas flow rate = 14 L min^{-1})

pure argon. Since it is a molecular gas with a strong bond energy, it absorbs a large amount of energy during the dissociation process, and the release of this energy by recombination reactions enhances the heat transfer between the cold gas and the arc column. The arc voltage of pure nitrogen is about twice that of the pure argon at the same gas flow rate. Figure 8 shows a comparison of the arc voltage and plasma jet length for two mixtures of nitrogen and argon, with 80% (Fig. 8a) and 70% (Fig. 8b) nitrogen by volume. The working voltages for the 80% nitrogen working gas were found to be higher for all currents.

Arc Voltage–Current Characteristics for Different Gas Flow Rates

The measured voltage–current characteristics for different gas flow rates are shown in Fig. 9. The arc voltage generally increases with both the gas flow rate and arc current. The minimum voltage of the laminar plasma torch was larger than 135 V. However, with an increase in arc current from 60 to 165 A, the increase in voltage was just 10 ± 2 V for all gas flow rates. As was shown in Fig. 6, the voltage fluctuation values were confined to the range of ± 0.5–2 V. Both the rate of change of voltage with current and the voltage fluctuations are much lower than those of conventional current non-transferred arc plasma torches

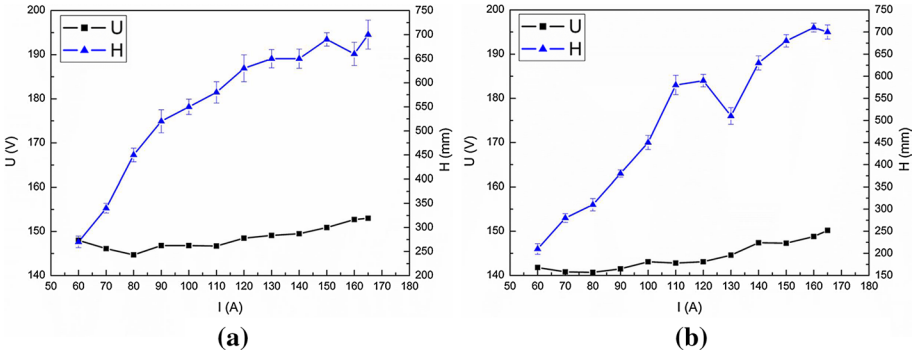

Fig. 8 Variation of laminar plasma jet length and arc voltage for a gas flow rate of 8.5 L min^{-1}, **a** for N_2:Ar = 8:2 by volume; **b** for N^2:Ar = 7:3 by volume

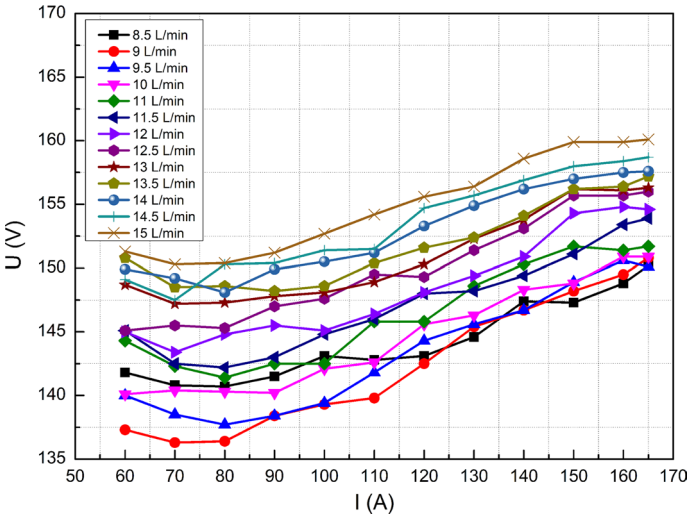

Fig. 9 Voltage–current characteristics of the laminar plasma torch at different gas flow rates for a mixture of 70% nitrogen and 30% argon by volume

(25–65 kW), which are operated at high current (usually 400–800 A), lower working voltage (usually 30–80 V) and have higher levels of voltage fluctuation (ΔU = ±5–25 V) [2, 4, 5, 7].

Initially, at a relatively low current (from around 60 to 70 A), the arc voltage decreases slightly with increasing current. This is because the arc temperature increases and the arc expands rapidly, so the electrical conductivity averaged over a radial cross-section of the arc increases. As the current increases further, the arc diameter remains approximately constant, and the electric conductivity increases less rapidly than the current. The voltage is approximately constant for a small range of currents, and then increases as the current continues to increase from about 80 A to 165 A. The voltage–current curve has an approximate U-shape over a large portion of its range. This behaviour is opposite to that of conventional direct current non-transferred arc plasma torches with a linear channel structure, such as the Sulzer PTF4 Gun, 3 MB Gun and Praxair SG-100 Gun, which exhibit

voltage–current curves with a drooping shape at the same level of output power [4, 5]. Moreover, the rising voltage–current characteristic enables the power supply to maintain an electrical efficiency close to unity. It is worth noting that the same rising voltage–current characteristics can be obtained in other laminar plasma torches that with very different inner channel structures: those of Osaki et al. [38], Pan et al. [14], M. F. Zhukov et al. (2003) [8, 39], Vilotijevic et al. [40] and Wang et al. [41].

Modelling of the Long Laminar Plasma Jet

Computational fluid dynamics modelling was performed to obtain greater understanding of the flow and heat transfer characteristics of the laminar plasma jet. A two-dimensional axisymmetric steady-state modelling approach was applied in this study. The model is constituted by the governing equations of conservation of mass, momentum and energy, and is implemented in the commercial software package ANSYS-Fluent v16.0. The simulations used was the pressure-based solver, the SIMPLE algorithm, and second order upwind differencing. The model assumes that the plasma is in Local Thermodynamic Equilibrium (LTE).

The governing equations are:

$$\frac{\partial}{\partial x}(\rho u) + \frac{1}{r}\frac{\partial}{\partial r}(r\rho v) = 0 \tag{1}$$

$$\frac{\partial(\rho uu)}{\partial x} + \frac{1}{r}\frac{\partial(r\rho uv)}{\partial r} = -\frac{\partial P}{\partial x} + 2\frac{\partial}{\partial x}\left(\mu_{eff}\frac{\partial u}{\partial x}\right) + \frac{1}{r}\frac{\partial}{\partial r}\left[r\mu_{eff}\left(\frac{\partial u}{\partial r} + \frac{\partial v}{\partial x}\right)\right] \tag{2}$$

$$\frac{\partial(\rho uv)}{\partial x} + \frac{1}{r}\frac{\partial(r\rho vv)}{\partial r} = -\frac{\partial P}{\partial r} + \frac{2}{r}\frac{\partial}{\partial r}\left[r\mu_{eff}\frac{\partial v}{\partial r}\right] + \frac{\partial}{\partial x}\left[\mu_{eff}\left(\frac{\partial v}{\partial x} + \frac{\partial u}{\partial r}\right)\right] - 2(\mu + \mu_t)\frac{v}{r^2} \tag{3}$$

$$\rho C_p\left(u\frac{\partial T}{\partial u} + \frac{1}{r}\frac{\partial v}{\partial r}\right) = \nabla\cdot(\kappa_{eff}\nabla T) - 4\pi\varepsilon_r \tag{4}$$

$$\rho\left(u\frac{\partial k}{\partial x} + v\frac{\partial k}{\partial r}\right) = \nabla\cdot(\alpha_k\mu_{eff}\nabla k) + G_k - \rho\varepsilon - Y_M \tag{5}$$

$$\rho\left(u\frac{\partial \varepsilon}{\partial x} + v\frac{\partial \varepsilon}{\partial r}\right) = \nabla\cdot(\alpha_\varepsilon\mu_{eff}\nabla\varepsilon) + C_{1\varepsilon}G_k\frac{\varepsilon}{k} - C_{2\varepsilon}\rho\frac{\varepsilon^2}{k} - R_\varepsilon \tag{6}$$

In these equations, u and v are the axial (x) and radial (r) velocity components; ρ, μ, k, C_p, and $4\pi\varepsilon_r$ are the plasma density, viscosity, thermal conductivity, specific heat at constant pressure, and radiated power per unit volume of plasma, respectively.

The Renormalization Group k-ε Model (RNG) was used for modelling turbulent viscosity in this study [42]. The RNG theory provides an analytically-derived differential formula for effective viscosity that accounts for low Reynolds-number effects, and an analytical formula for turbulent Prandtl numbers, while the standard k-ε model uses user-specified constant values. These features make the RNG k-ε model more accurate and reliable for a wide class of flows than the standard k-ε model, especially in the case of the laminar plasma jet considered here.

In Eqs. (5) and (6), G_k represents the generation of turbulent kinetic energy due to the mean velocity gradients, and Y_M represents the contribution of the fluctuating dilatation in compressible turbulence to the overall dissipation rate [42]. The quantities α_k and α_ε, respectively the inverse effective Prandtl numbers for k and ε are both set equal to 1.393. $C_{1\varepsilon}$ and $C_{2\varepsilon}$ are set equal to 1.42 and 1.68 respectively. The main difference between the RNG and the standard k-ε model lies in the additional term of the turbulent dissipation equation given by:

$$R_\varepsilon = \frac{C_\mu \rho \eta^3 (1 - \eta/\eta_0)}{1 + \beta \eta^3} \cdot \frac{\varepsilon^2}{k} \tag{7}$$

where η_0=4.38, β=0.012, C_μ=0.0845. The effective viscosity is given by:

$$\mu_{eff} = \mu + \mu_t \tag{8}$$

$$\mu_t = \rho C_\mu \frac{k^2}{\varepsilon} \tag{9}$$

For the case of laminar flow simulations, Eqs. (1) to (4) were used by setting the turbulent viscosity μ_t equal to 0 and Eqs. (5) and (6) were removed from the model. The effective viscosity option in the RNG Model was used in the simulation. This allows modelling of the effective turbulent transport variation with the effective Reynolds number (or eddy scale), allowing the model to better handle low- Reynolds- number and near- wall flows [42].

Actually, authors have tried Standard k-ε Model, k-omega Model, Reynolds Stress Model and Spalart–Allmaras Model to simulate this plasma jet. These results list in the supplement files. However, these results are all far away from the experiment observations.

The computational domain is shown in Fig. 10; the diameter of the nozzle exit is 5 mm, and the values of the other boundary conditions are shown in Table 1. The initial flow inlet conditions (AB) were derived from the results of modelling of the internal regions of the laminar plasma torch (Fig. 11) [36], for operation at 25.4 kW (for a total current of 160 A) in 70% nitrogen and 30% argon by volume, with a total flow rate of 14 L min^{-1}. The maximum velocity and temperature at the inlet are respectively 2024 m/s and 16 870 K. The boundary BC is the water-cooled wall of the torch nozzle, for which the thermal boundary conditions is specified by a heat transfer coefficient (h_w) of 1.0×10^5 W $m^{-2}K^{-1}$ and reference cooling water temperature (T_w) of 500 K.

The thermodynamic and transport properties of nitrogen and argon mixtures were calculated using the methods presented in references [43] and [44]. The data used in the

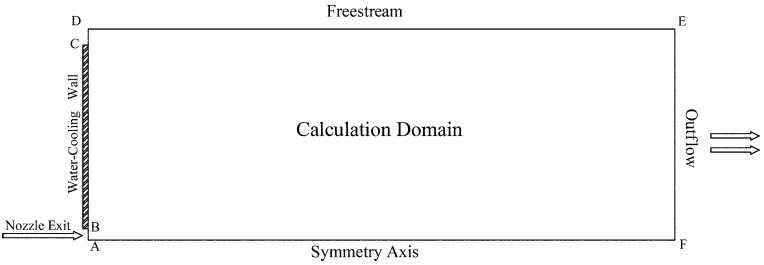

Fig. 10 Schematic of the computational domain of the laminar plasma jet model

Table 1 Boundary conditions of the computational domain

Defined condition	Boundary	T (K)	V (m s^{-1})	S (mm)
Nozzle exit	AB	Fig. 11b	Fig. 11a	2.5
Nozzle wall	BC	$h_w\,(T-T_w)$	0	37.5
Freestream	CD	300	–	10
Freestream	DE	300	–	400
Symmetry axis	AF	–	–	400
Outflow	EF	–	–	50

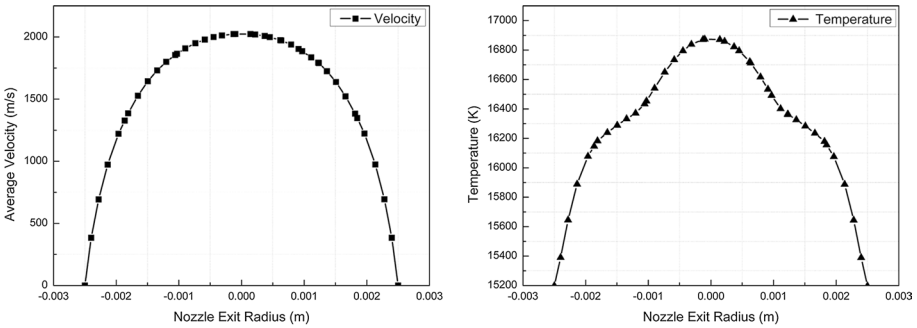

Fig. 11 Boundary conditions at the nozzle exit: **a** velocity and **b** temperature. Profiles obtained by a model of the internal region of the laminar plasma torch operating at 25.4 kW (I = 160 A, Q = 14 L min^{-1} with 70% nitrogen and 30% argon in volume)

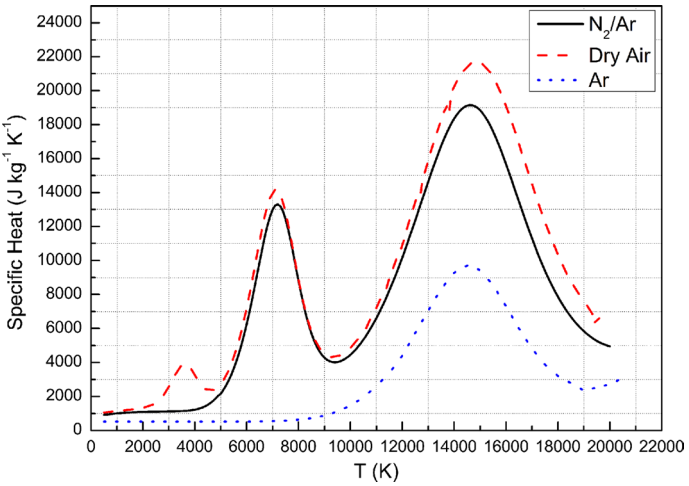

Fig. 12 Temperature dependence of the specific heat of dry air [46], argon [45] and the mixture of 70% nitrogen and 30% argon [36] used in this work at atmospheric pressure

model were presented in [36]. Figure 12 shows the temperature dependent of specific heat of dry air [45], argon [45] and the mixture of 70% nitrogen and 30% argon used in this work [36]. The model assumes that the discharge environment has the same composition as the working gas (i.e. argon–nitrogen mixture). This assumption significantly simplifies the model and is expected to be reasonable given the relatively small difference in specific heats between the Ar–N_2 mixtures used in the model and air for the characteristics of the plasma jet (i.e. temperature < 14,000 K).

Figure 13 shows the velocity and temperature distributions of the plasma jet obtained using the laminar flow model for operation at the output power of 25.4 kW (I = 160 A) using 70% nitrogen and 30% argon. The velocity of the plasma jet plume rapidly decreases downstream of the nozzle exit. The length of the jet for which the velocity remains greater than 1000 ms^{-1} is about 100 mm. The high temperature jet expands rapidly as it is ejected out of the nozzle exit. The temperature distribution showed a high-temperature vortex region at over 10,000 K very close to the nozzle exit before narrowing to form a uniform and slowly expanding jet. This is consistent with the experimental observation shown in Figs. 3a and 15 of the presence of a bright region close to the nozzle exit.

The velocity and temperature distributions presented by the RNG turbulent model are presented in Fig. 14. The results are very similar to those in Fig. 13. The high temperature region at the nozzle exit slightly decreased in size.

The attenuation of axial velocity and temperature along the jet axis obtained using the two models are shown in Fig. 15. The temperature at the torch exit was 16,870 K and decreased rapidly to below 8500 K within 5 mm of the nozzle exit. The attenuation of the axial velocity is less rapid. The RNG model predicts less rapid decreases of axial velocity

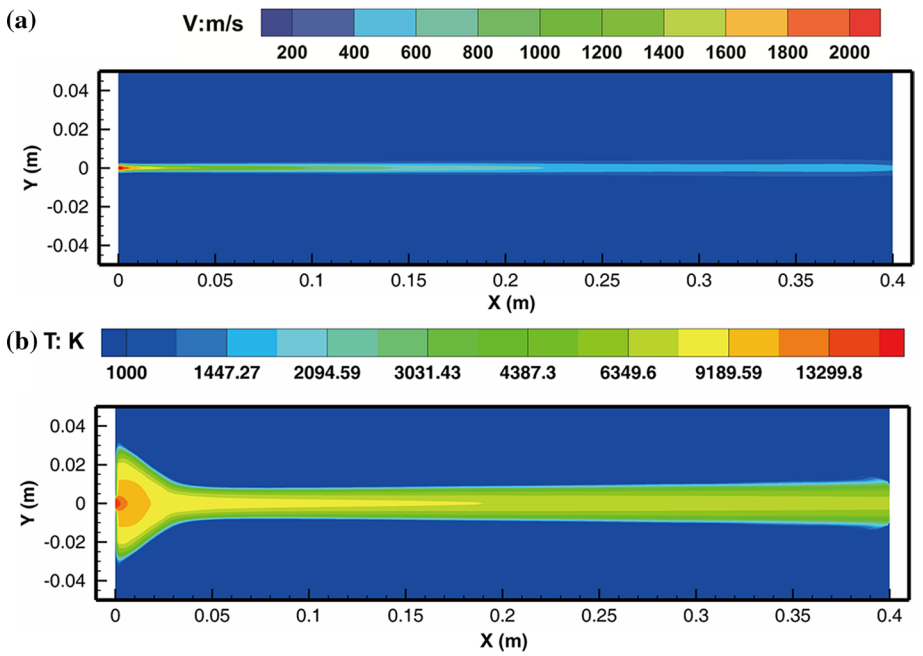

Fig. 13 Velocity and temperature distributions of the plasma jet predicted by the laminar model

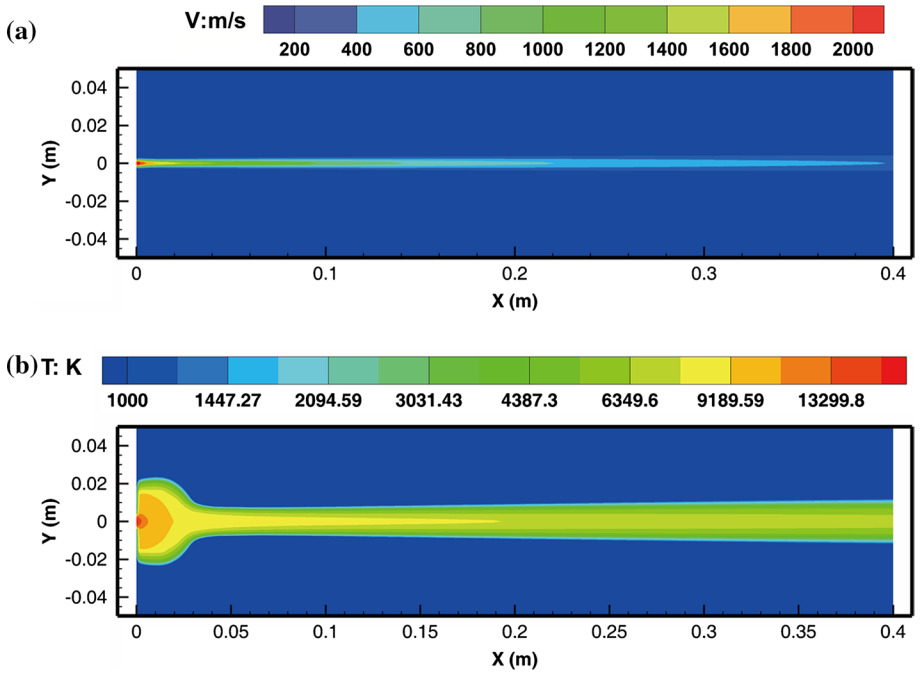

Fig. 14 Velocity and temperature distributions of the plasma jet predicted by the RNG turbulent model

and particularly temperature than the laminar model in the downstream regions, but the differences between the models are relatively small.

Figure 16 showed the turbulent dissipation, turbulent kinetic energy and turbulent intensity distributions. All three quantities are largest at the nozzle exit, where the velocity and temperature are largest. The turbulent energy is rapidly dissipated both radially and axially away from the exit. Similarly, the turbulent intensity continuously decreases along the direction of flow. The distribution of turbulence intensity differs strongly from that of conventional direct-current non-transferred arc plasma torch, in which a very high turbulence intensity occurs at the interface between the expanding plasma jet and the atmosphere [46, 47]. This region of strong turbulence leads to greatly enhanced mixing of the atmosphere into the plasma jet, leading to a rapid cooling of the jet. The absence of such strong turbulent mixing facilitates the formation of the long laminar plasma jets studied in this article.

Conclusions

This article presented the experimental and numerical study of a novel direct current non-transferred arc plasma torch that can generate different lengths of long laminar plasma jets in ambient air. The results showed that the long laminar plasma jets can be conveniently controlled through the gas flow rate and output power of the equipment. The experimental observations of the plasma jet indicated a high stability in the atmospheric environment. The maximum jet length can reach about 720 mm in air. An

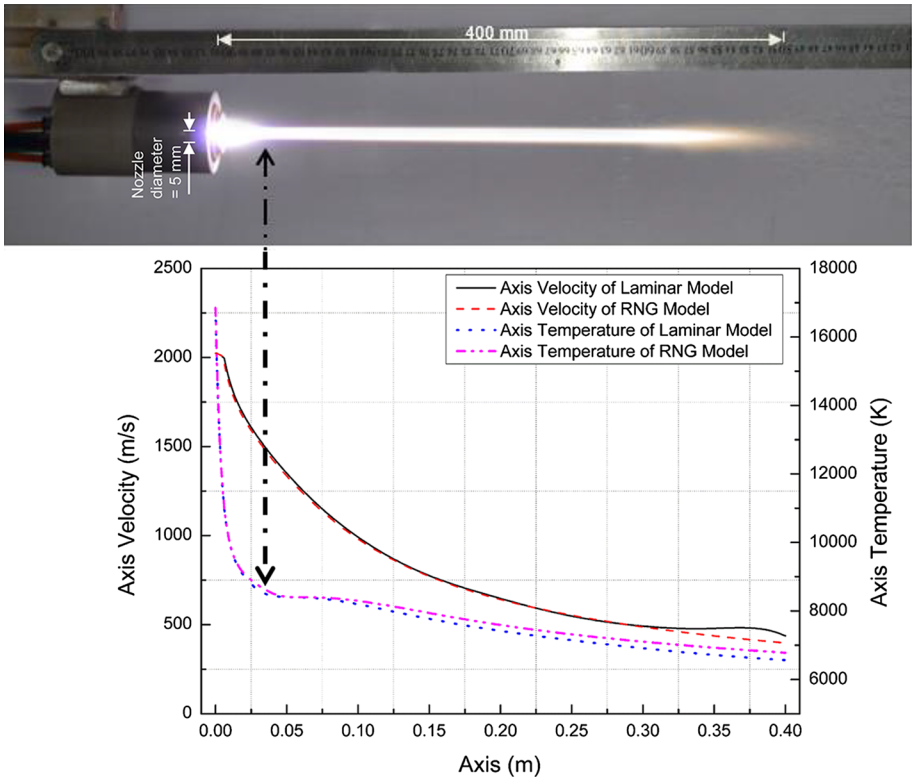

Fig. 15 Attenuation of the axial velocity and temperature along the plasma jet axis and comparing with the experimental observation

increasing voltage current characteristic was obtained under a gas flow rate of 8.5–15 L min^{-1} and a working current of 60–165 A, for operation with a mixture of 70% nitrogen and 30% argon by volume.

The flow characteristics of the long laminar plasma jet were studied using two-dimensional computational fluid dynamics model that makes use of nozzle data produced by a coupled electromagnetic and fluid dynamic model of the plasma inside the body of the torch. A bright region near the nozzle exit that was observed in the experiments corresponds to a region predicted to be at the temperature of over 10,000 K; the temperature was predicted to rapidly decrease downstream of the bright region. The attenuation of velocity along the torch axis was smaller than that of temperature. The turbulent kinetic energy and intensity were predicted to be highest near the nozzle exit. This is in contrast to conventional plasma torches, in which they are largest in the regions at the interface between the expanding plasma jet and the atmosphere.

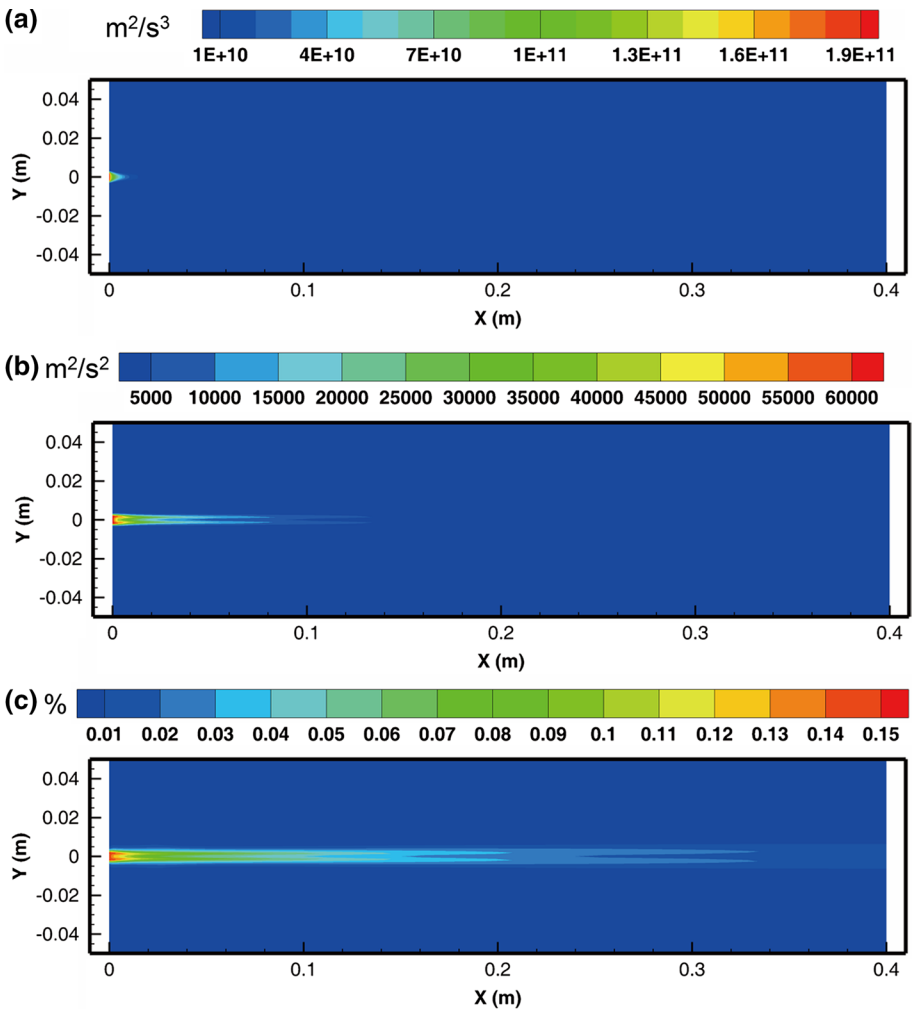

Fig. 16 Turbulent dissipation ($m^2\ s^{-3}$), turbulent kinetic energy ($m^2\ s^{-2}$), and turbulent intensity (%) distributions of the plasma jet

Acknowledgements The authors are grateful to Prof. Ren-zhong Huang from the Department of New Materials of Guangzhou Non-Ferrous Metal Research Institute for his selfless help with the computer programming. This work was supported by the Natural Key R&D Program of China (Basic Research Project, Grant No. 2017YFB0306104), the Ph.D. Short-term Academic Visiting Program of Graduate School of Xi'an Jiaotong University and National Ph.D. Degree Program of the China Scholarship Council.

References

1. Zhukov MF, Zasypkin IM (2006) Thermal plasma torches—design, characteristics, applications. Cambridge International Science Publishing, pp 1–15
2. Fauchais P (2004) Understanding plasma spraying. J Phys D Appl Phys 37(9):R86–R108. https://doi.org/10.1088/0022-3727/37/9/R02

3. Fauchais PL, Heberlein JVR, Boulos MI (2014) Thermal spray fundamentals. Springer. https://doi.org/10.1007/978-0-387-68991-3
4. Coudert JF, Rat V, Rigot D (2007) Influence of Helmholtz oscillations on arc voltage fluctuations in a dc plasma spraying torch. J Phys D Appl Phys 40(23):7357–7366. https://doi.org/10.1088/0022-3727/40/23/016
5. Nogues E, Vardelle M, Fauchais P, Granger P (2008) Arc voltage fluctuations: comparison between two plasma torch types. Surf Coat Technol 202(18):4387–4393. https://doi.org/10.1016/j.surfcoat.2008.04.014
6. An LT, Gao Y, Sun C (2011) Effects of anode arc root fluctuation on coating quality during plasma spraying. J Therm Spray Technol 20(4):775–781. https://doi.org/10.1007/s11666-011-9644-y
7. Janisson S, Vardelle A, Coudert JF, Fauchais P, Meillot E (1999) Analysis of the stability of dc plasma gun operating with Ar–He–H_2, gas mixtures. Ann N Y Acad Sci 891(1):407–416
8. Solonenko OP (ed) (2003) Thermal plasma torches and technologies: plasma torches, basic studies and design. Cambridge international science publishing, pp 9–12
9. Solonenko OP, Nishiyama H, Smirnov AV, Takana H, Jang J (2014) Visualization of arc and plasma flow patterns for advanced material processing. J Vis 18:1–15. https://doi.org/10.1007/s12650-014-0221-6
10. Hideki Hamatani FW (2016) Development of laminar plasma shielded HF-ERW process—advanced welding process of HF-ERW 3. In: Proceedings of the 2012 9th international pipeline conference (pp 1–8)
11. Hamatani H, Ohara M, Fuji M (1999) Development of high power hybrid plasma spraying. J Japanese Inst Met 63(1):135–143. http://ci.nii.ac.jp/naid/10002548732/en/. (**in Japanese**)
12. Ma W, Pan WX, Wu CK (2005) Preliminary investigations on low-pressure laminar plasma spray processing. Surf Coat Technol 191(2–3):166–174. https://doi.org/10.1016/j.surfcoat.2004.02.011
13. Ma W (2006) Influence of the processing conditions on the characteristics of the clad layers produced with laminar plasma technology. Appl Surf Sci 252(23):8352–8359. https://doi.org/10.1016/j.apsusc.2005.11.043
14. Pan WX, Zhang W, Zhang W, Wu C (2001) Generation of long, laminar plasma jets at atmospheric pressure and effects of flow turbulence. Plasma Chem Plasma Process 21(1):23–35
15. Pan WX, Meng X et al (2008) Experimental observations on the stability and 3-D characteristics of laminar/turbulent plasma jets. J Eng Thermophys 29(1):2–4 **(in Chinese)**
16. Pan WX (2006) Arc voltage fluctuation in dc laminar and turbulent plasma jets generation. Plasma Sci Technol 416(4)
17. Meng X, Pan W, Chen X, Guo Z, Wu C (2011) Temperature measurements in a laminar plasma jet generated at reduced pressure. Vacuum 85(7):734–738. https://doi.org/10.1016/j.vacuum.2010.11.007
18. Meng X, Pan WX, Wu CK (2004) Temperature and velocity measurement of laminar plasma jet. J Eng Thermophys 24(3):5–7 **(in Chinese)**
19. Meng X, Pan WX, Wu CK (2005) Transient measurement and analysis on heat flux distributions of partially-ionized high-temperature laminar flow jet. J Eng Thermophys 26(1):137–139 **(in Chinese)**
20. Cheng K, Chen X, Pan WX (2005) Efforts of shroud gas on laminar argon plasma jets impinging on a substrate in ambient air. J Eng Thermophys 26(6):1–3 **(in Chinese)**
21. Zhang WWX et al (1999) Modelling of laminar plasma jet impinging on a flat plate with approximate box relaxation method. Plasma Sci Technol 1:1
22. Wang HX, Xi C, Pan WX, Kai C (2007) Comparison of the characteristics of laminar and turbulent impinging plasma jets. J Eng Thermophys 28(4):7–9 **(in Chinese)**
23. Wang H-X, Chen X, Cheng K, Pan W (2007) Modeling study on the characteristics of laminar and turbulent argon plasma jets impinging normally upon a flat plate in ambient air. Int J Heat Mass Transf 50(3–4):734–745. https://doi.org/10.1016/j.ijheatmasstransfer.2006.07.002
24. Cheng K, Chen X, Wang H-X, Pan W (2006) Modeling study of shrouding gas effects on a laminar argon plasma jet impinging upon a flat substrate in air surroundings. Thin Solid Films 506–507:724–728. https://doi.org/10.1016/j.tsf.2005.08.148
25. Pan WMX (2007) Comparative observation of Ar, Ar–H_2 and Ar–N_2 DC arc plasma jets and their arc root behaviour at reduced pressure. Plasma Sci Technol 9:2
26. Peng Y (2012) Numerical simulation study on flow fields in a non-transferred direct current plasma generator operating at reduced pressure. M. D. thesis, Institute of Mechanics, China Academy of Science
27. Xu DY (2003) Studies of long laminar plasma jet generation and characteristics. Ph.D. thesis, Tsinghua University

28. Wang Hai-Xing, Chen Xi, Pan Wenxia (2007) Modeling study on the entrainment of ambient air into subsonic laminar and turbulent argon plasma jets. Plasma Chem Plasma Process 27(2):141–162. https://doi.org/10.1007/s11090-006-9047-x
29. Wang H-X, Chen X, Pan W (2007) Effects of the length of a cylindrical solid shield on the entrainment of ambient air into turbulent and laminar impinging argon plasma jets. Plasma Chem Plasma Process 28(1):85–105. https://doi.org/10.1007/s11090-007-9109-8
30. Xu D-Y, Chen X, Pan W (2005) Effects of natural convection on the characteristics of a long laminar argon plasma jet issuing horizontally into ambient air. Int J Heat Mass Transf 48(15):3253–3255. https://doi.org/10.1016/j.ijheatmasstransfer.2005.02.039
31. Xu D-Y, Chen X, Cheng K (2003) Three-dimensional modelling of the characteristics of long laminar plasma jets with lateral injection of carrier gas and particulate matter. J Phys D Appl Phys 36(13):1583–1594
32. Huang H, Pan W, Guo Z, Wu C (2008) Laminar/turbulent plasma jets generated at reduced pressure. IEEE Trans Plasma Sci 36(4):1052–1053
33. Duan Z, Heberlein J (2002) Arc instabilities in a plasma spray torch. J Therm Spray Technol 44–51
34. Liu SH, Li CX, Zhang SH et al (2018) A novel structure of YSZ coatings by atmospheric laminar plasma spraying technology. Scr Mater 153:73–76
35. Liu SH, Li CX et al (2018) Development of long laminar plasma jet on thermal spraying process: microstructures of zirconia coatings. Surf Coat Technol 337:241–249
36. Liu S-H, Li C-X, Murphy AB, Li CJ (2018) Numerical simulation of the flow characteristics inside a novel plasma spray torch. Plasma Chem Plasma Process (under review)
37. Mohanty P, Stanisic J, Stanisic J, George A, Wang Y (2010) A study on arc instability phenomena of an axial injection cathode plasma Torch. J Therm Spray Technol 19(1–2):465–475. https://doi.org/10.1007/s11666-009-9444-9
38. Osaki K, Fukumasa O, Kobayashi A (2000) High thermal efficiency-type laminar plasma jet generator for plasma processing. Vacuum 59:47–54
39. Solonenko OP, Zhukov MF (eds) (1994) Thermal plasma and new materials technology vol 1 investigation and design of thermal plasma generators. Cambridge Interscience Publishing, pp 5–43
40. Vilotijevic M, Dacic B, Bozic D (2009) Velocity and texture of a plasma jet created in a plasma torch with fixed minimal arc length. Plasma Sources Sci Technol 18(1):15016. https://doi.org/10.1088/0963-0252/18/1/015016
41. Wang JL (2015) Investments of mental rapid manufacturing by laminar plasma torch. University of Science and Technology of China, M.D. dissertation. (**In Chinese**)
42. ANSYS Inc. (2016) ANSYS fluent theory guide. USA
43. Cram LE (1985) Statistical evaluation of radiative power losses from thermal plasmas due to spectral lines. J Phys D Appl Phys 18(3):401–411. https://doi.org/10.1088/0022-3727/18/3/009
44. Murphy AB, Arundelli CJ (1994) Transport coefficients of argon, nitrogen, oxygen, argon-nitrogen, and argon-oxygen plasmas. Plasma Chem Plasma Process 14(4):451–490. https://doi.org/10.1007/BF01570207
45. Boulos M, Fauchais P, Pfender E (1994) Thermal plasmas: fundamentals and applications. Springer
46. Pfender E, Fincke J, Spores R (1991) Entrainment of cold gas into thermal plasma jets. Plasma Chem Plasma Process 11(4):529–543
47. Murphy AB, Kovitya P (1993) Mathematical model and laser-scattering temperature measurements of a direct-current plasma torch discharging into air. J Appl Phys 73(10):4759–4769. https://doi.org/10.1063/1.353840